

DeepGraviLens: a Multi-Modal Architecture for Classifying Gravitational Lensing Data

Nicolò Oreste Pinciroli Vago , Piero Fraternali 

Abstract—Gravitational lensing is the relativistic effect generated by massive bodies, which bend the space-time surrounding them. It is a deeply investigated topic in astrophysics and allows validating theoretical relativistic results and studying faint astrophysical objects that would not be visible otherwise. In recent years Machine Learning methods have been applied to support the analysis of the gravitational lensing phenomena by detecting lensing effects in data sets consisting of images associated with brightness variation time series. However, the state-of-art approaches either consider only images and neglect time-series data or achieve relatively low accuracy on the most difficult data sets. This paper introduces DeepGraviLens, a novel multi-modal network that classifies spatio-temporal data belonging to one non-lensed system type and three lensed system types. It surpasses the current state of the art accuracy results by $\approx 19\%$ to $\approx 43\%$, depending on the considered data set. Such an improvement will enable the acceleration of the analysis of lensed objects in upcoming astrophysical surveys, which will exploit the petabytes of data collected, e.g., from the Vera C. Rubin Observatory.

Index Terms—Multimodal Deep Learning, Multimodal Network, Fusion, Gravitational Lensing, Supernovae, Time series.

I. INTRODUCTION

IN astrophysics, a gravitational lens is a matter distribution (e.g., a black hole) able to bend the trajectory of transiting light, similar to an optical lens. Such apparent distortion is caused by the curvature of the geometry of space-time around the massive body acting as a lens, a phenomenon that forces the light to travel along the geodesics (i.e., the shortest paths in the curved space-time).

Strong and weak gravitational lensing focus on the effects produced by particularly massive bodies (e.g., galaxies and black holes), while microlensing addresses the consequences produced by lighter entities (e.g., stars). Strong lensing is involved in major astrophysical problems: studying massive bodies that are too faint to be analyzed with current instrumentation; characterizing the geometry, content and kinematics of the universe; and investigating mass distribution in the galaxy formation process [64]. Discovery is only the first step, yet a fundamental one, in the study of gravitational lenses. Finding evidence of strong gravitational lensing enables the validation and the advancement of existing astrophysical theories, such as the theory of general relativity [53], and supports specialized studies aimed at modeling the effects of gravitational lensing on specific entities, such as wormholes [53], Simpson-Visser black holes [26], and Einstein-Gauss-Bonnet black holes [29].

The authors are with the Department of Electronics, Information and Bioengineering, Politecnico di Milano, 20133 Milan, Italy (e-mail: nicolo.oreste.pinciroli@polimi.it; piero.fraternali@polimi.it).

The gravitational lenses discovery task takes as input spatio-temporal observations consisting of images and time series and associates each observation with one class (e.g., “Lens”, “No lens”, “Lensed galaxy”...). Images are obtained from specific regions of the electromagnetic field (e.g., visible and infrared [11], ultra-violet [48], and green, red, and near-infrared [41]), depending on the specific experiment. Time series are also collected in specific electromagnetic field regions. They typically describe brightness variation through time (e.g. [41], [66]), and their sampling frequency depends on the technological constraints of the acquisition instrument. In general, they can be multivariate time series [45], [46]. Observations can be either real (i.e., collected by actual instruments) or simulated (i.e., generated by a software system that replicates the characteristics of real instruments).

As [26], [29], [53], [64] show, gravitational lensing systems can be complex, ubiquitous and hard to detect without computer-aided data processing. The volumes of data gathered by contemporary instruments make manual inspection unfeasible. As an example, the Vera C. Rubin Observatory is expected to collect petabytes of data [68].

Several gravitational lenses discovery approaches and tools have been introduced in the past. Originally, observations were analyzed without the aid of computers [75]. Even after the advent of computer science, observations were initially processed without automated classification systems [21], [31], [65]. More recently, Machine Learning (ML) methods have been exploited. The works [12], [61] use Convolutional Neural Network (CNNs) to classify gravitational lensing images, [40] exploits a Bayesian approach to categorize image data, and [41] applies a multi-modal approach to classify spatio-temporal data in four simulated data sets generated by the deepastronomy simulator [42]. In particular, [41] classifies gravitational lensing data by applying a CNN to the image and a Long Short-Term Memory (LSTM) network to the brightness time series and then fusing the outputs of the two branches, achieving a test accuracy ranging from 48.7% to 78.5%.

State-of-the-art lens detection systems, however, still present several limitations. Some of them (e.g., [12], [40], [61]) rely on images only and neglect time-domain data. [41], instead, considers spatio-temporal simulated data but shows relatively low accuracy on the most challenging data sets.

This paper introduces DeepGraviLens, a novel architecture for the classification of strong gravitational lensing multi-modal data. The contributions can be summarized as follows

- We introduce the architecture of DeepGraviLens, which takes in input spatio-temporal data simulating astrophysical observations and produces in output a multi-

class single-label classification of each spatio-temporal sample. DeepGraviLens exploits three complementary sub-networks trained independently and combines their outputs by means of a fully connected final stage. The three sub-networks apply different and complementary ways of combining image and time-series data, taking advantage of both the local and the global features of the input data.

- We evaluate the designed architecture on four data sets and compare its predictions to the results obtained by the DeepZipper network [41]. DeepGraviLens yields accuracy improvements ranging from $\approx 19\%$ to $\approx 43\%$ and significantly reduces the confusion between similar classes, one of the major issues of gravitational lenses classification.

The obtained improvements in the classification of lensing phenomena will enable a faster and more accurate characterization of future real observations, such as those of the Vera C. Rubin Observatory, and will open the way to the discovery of lensed supernovae, which are among the hardest bodies to detect due to their rarity, scattered spatial distribution and relatively short observable life [13], [20], [27], [43], [71].

The rest of this paper is organized as follows: Section II surveys the related work; Section III describes the data set and the architecture of DeepGraviLens; Section IV describes the adopted evaluation protocol and presents quantitative and qualitative results; finally, Section V draws the conclusions and outlines our future work,

II. RELATED WORK

This section surveys the previous research in the fields of automated gravitational lensing analysis and multi-modal Deep Learning, which are the foundations of this work.

A. Automated Gravitational Lensing Analysis

Classifying gravitational lensing phenomena is a challenging task and the subject of many studies. This section concentrates on the data-driven techniques, as opposed to the analytical methods that focus on the design of mathematical models capable of explaining the observed data.

The work described in [40] applies a Bayesian approach to classify high-resolution images to reproduce the categorization performed by human experts. However, high-resolution images are not always available and the human classification (“Definitely not a lens”, “Possibly a lens”, “Probably a lens”, “Definitely a lens”) is intrinsically imprecise and prone to bias depending on the human classifier.

The approach discussed in [22] aims at separating lensed and non-lensed systems using an SVM, whose output is then compared to an assessment of the same images performed by human experts. The use of an SVM requires a feature extraction and selection step based on experts’ knowledge.

The binary classifiers introduced in [12] and in [47] also aim at separating lensed and non-lensed systems but exploit a CNN applied to simulated images and wide-field survey data. As with the previous methods, no time-domain information is

considered and no fine-grain classification of lensed systems is performed.

Differently from previous approaches, DeepZipper [41] casts the problem as a multi-class single-label classification task for data sets consisting of images associated with time series of brightness variation. To analyze both images and time-series data, the authors propose a multi-modal network, formed by a CNN and an LSTM, whose outputs are then fused. The resulting system is applied to four simulated data sets, each corresponding to a different astronomical survey (DES-wide, LSST-wide, DES-deep, and DESI-DOT). This approach, although relatively simple, achieves good results on all four data sets, with accuracies ranging from 48.7% to 78.5%.

B. Multi-modal Deep Learning and Fusion

Several phenomena in the most varied disciplines are characterized by heterogeneous data that give complementary information about the subject under investigation. Multi-modal DL has proved its effectiveness in those domains that require the integrated analysis of multiple data types (e.g., images, videos and time series). The survey in [50] overviews the advances and the trends in multi-modal DL until 2017 and documents usage in such areas as medicine [4], [6], [33], human-computer interaction [3] and autonomous driving [18], [38]. The recent survey [58] discusses several applications combining image and text [35], [36], video and text [37], [49], and text and audio [14], [54]. Some applications rely on physiological signals for behavioral studies, such as face recognition [9], [28], [32]. In the medical field, [55] overviews the use of AI in oncology and shows the benefits of multi-modal DL. The work in [72] diagnoses cervical dysplasia with the integrated analysis of images and numerical data. [19] employs multi-modal DL for classifying malware using textual data from different sources. [67] exploits images and texts to detect hate speech in memes. [51] uses multiple robotic sensors (e.g., cameras, tactile and force sensors) for object manipulation.

From the architecture viewpoint, the processing of heterogeneous inputs can be performed by analyzing the individual data types separately and then fusing the outcome of the different branches to produce an output (late fusion), by stacking the inputs, which are processed together (early fusion), or by introducing fusion at a middle stage (intermediate fusion) [50], [56]. The survey [17] overviews DL methods for multi-modal data fusion in general whereas [56] focuses on biomedical data fusion. The work in [58] broadens the comparison beyond DL and contrasts alternative methods employed in multi-modal classification tasks, including SVMs [25], RNNs [28], [69], CNNs [23], [44] and even GANs [70].

DeepGraviLens introduces a novel approach for the classification of images and time series representing simulated lensed astrophysical objects. The proposed architecture exploits three multi-modal networks whose results are fused using ReFuse, a Fully Connected network: LoNet exploits late fusion and emphasizes the local features of the image; GloNet applies early fusion and accentuates the global features of both types of input; MuNet employs late fusion but extracts both local and global features from the image.

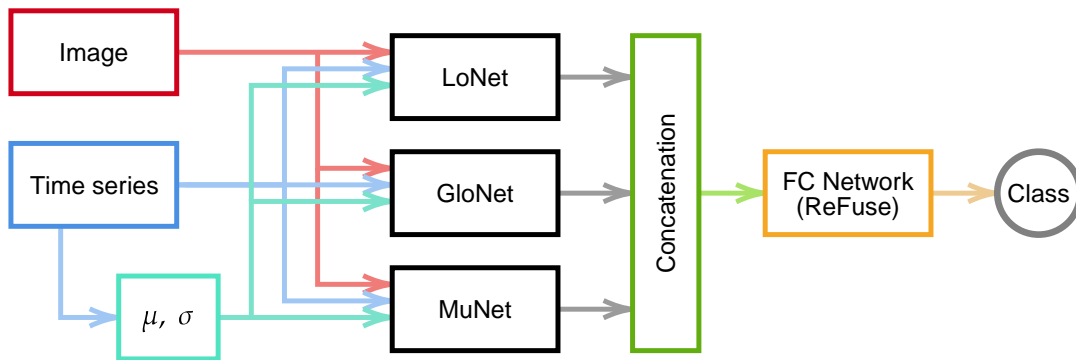


Fig. 1. The DeepGraviLens pipeline comprises four steps: (1) the inputs are fed into three independent networks (LoNet, GloNet, and MuNet); (2) the outputs of the three networks are concatenated; (3) the ReFuse network receives the concatenated outputs and (4) outputs a predicted class.

III. DATA SETS AND METHODS

A. Datasets

An input to the lensed object classification task consists of four images and four brightness variation time series, which together represent an astrophysical observation. One image and one time series are provided for each band of the *griz* photometric system, widely used in CCD cameras [52]. In this system, the g band is centered on green, the r band is centred on red, the i band is the near-infrared one, and the z band is the infrared one.

Each input is labeled with one of four classes: “No Lens” (no lensed system), “Lens” (Galaxy-Galaxy lensing), “LSNIa” (the lensed object is a Type-Ia supernova), and “LSNCC” (the lensed object is a core-collapse supernova). Section IV-B shows various examples of input samples and of their classification by DeepGraviLens.

Four distinct data sets (DESI-DOT, LSST-wide, DES-wide, and DES-deep) are built via simulation and are used for training and evaluating DeepGraviLens. The details of their construction are explained in [5], [41], [42]. Each data set simulates a current or next-generation cosmic survey and is characterized by different specifications of the images and of the associated time series.

The DESI-DOT data set simulates the observations made by the Dark Energy Camera (DECam) [16] and mirrors the real observing conditions of the DES wide-field survey reported in [1]. The exposure time, a simulation parameter that affects the image quality (higher is better), was set to 60 seconds. The LSST-wide data set simulates the LSST survey images acquired using the LSSTCam camera [57]. The simulation parameters were estimated from the conditions of the first year of the survey and the exposure time was set to 30 seconds [39]. The DES-wide data set emulates the images from the DECam and uses the real observing conditions from the DES wide-field survey, but the exposure time is 90 seconds. The DES-deep data set also reproduces the images from DECam but its characteristics are simulated according to the DES SN program [2] with the exposure time set to 200 seconds.

Due to the use of the four-bands *griz* photometric system, each image has 4 layers. The image size is $45 \times 45 \times 4$ pixels for all the four data sets. The length of the time series depends

on the technical limitations of the simulated instruments. DESI-DOT, LSST-wide, and DES-deep time series contain 14 samples for each band, while DES-wide contains 7 samples for each band.

For each data set, 17 astrophysical systems were defined and grouped into the four classes “No Lens”, “Lens”, “LSNIa”, and “LSNCC”. The examples of the four classes were generated randomly: each class covers $\approx 25\%$ of each data set and the distribution of the 17 subsystems is the same in all the data sets. Each data set comprises $\approx 40,000$ elements, split into the train set ($\approx 81\%$), the validation set ($\approx 9\%$), and the test set ($\approx 10\%$).

B. Extraction of statistical quantities

Two statistical quantities (mean and standard deviation) are extracted from the brightness time series and added as inputs to DeepGraviLens. Such derived data have a physical meaning. For example, an empty sky is expected to have approximately the same mean value for the four bands and a high standard deviation (because the fluctuations are random). A non-lensed star is expected to be characterized by a low standard deviation, as the means are approximately constant. Even when they manifest a transient behavior (e.g., the explosion of a supernova), the brightness variation is attenuated by the distance. Lensed bodies instead are expected to have a higher standard deviation, because when they display a transient behavior their brightness is amplified by the lens. The contribution of such derived inputs is quantified in the ablation study described in Section IV.

C. Architecture

Figure 1 illustrates the two-stage multi-modal inference pipeline of DeepGraviLens. It is formed by three sub-networks (LoNet, GloNet, and MuNet), whose outputs are combined by the ReFuse Fully Connected sub-network. Table I summarizes the characteristics of the three networks. GloNet exploits the combination of the image and time-series data, which are merged using early fusion. This approach emphasizes the global features of the multi-modal inputs. LoNet focuses on the local features of the distinct data types: the image and the time series pass through two separate sub-networks and then

TABLE I

THE THREE SUB-NETWORKS PURSUE DIFFERENT GOALS: GLONET EMPHASIZES GLOBAL FEATURES AND APPLIES EARLY FUSION; LO.NET ACCENTUATES LOCAL FEATURES AND EMPLOYS LATE FUSION; MU.NET EXTRACTS BOTH GLOBAL AND LOCAL IMAGE FEATURES.

Data fusion	Feature extraction	Global	Local
	Early		GloNet
Late			LoNet
		MuNet	

late fusion is applied. Finally, MuNet extracts both local and global features from the image, using an FC sub-network and a CNN in parallel, and then applies late fusion.

D. LoNet, a network focusing on local features

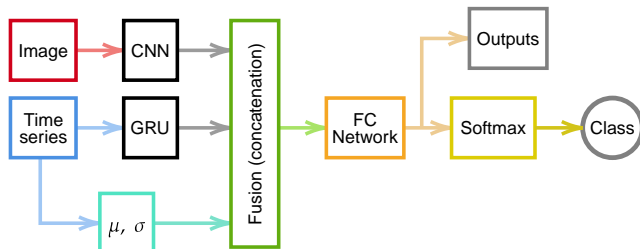


Fig. 2. **LoNet** architecture. The time series is processed by a GRU module and the image by a CNN. The two outputs together with the statistics are fused and fed as input to a FC module.

Figure 2 shows the architecture of the LoNet sub-network and Table II summarizes its features. It comprises two branches, one for the image (processed through a CNN) and one for the time series (processed by a GRU module). This structure is similar to the one of ZipperNet [41] but replaces the LSTM [24] module with a GRU module with a smaller hidden unit size [7]. The benefits of GRU over LSTM have been shown in several applications [8], [10], [30], [60], [73]. In the considered data sets, the short length of the time series makes GRU advantageous over LSTM because the former has fewer training parameters and thus better generalization abilities. Since the DES-wide data set has shorter time series, the GRU’s hidden state size is set to 32 for DES-wide and 64 for the other data sets. This reduction has been frequently applied in the literature to limit the number of nodes and thus avoid overfitting [15], [34], [59].

The output of the CNN and of the GRU, the means and the standard deviations of the time series are concatenated and fed in input to a late fusion FC sub-network [56].

E. GloNet, a network focusing on global features

Figure 3 shows the architecture of the GloNet sub-network and Table III summarizes its features. GloNet, differently from

TABLE II

LO.NET ARCHITECTURE – THE † SYMBOL DENOTES THE USE OF RELU, WHILE THE ‡ SYMBOL DENOTES THE USE OF LOGSOFTMAX. IN THE LAST COLUMN, h DENOTES THE SIZE OF THE GRU HIDDEN STATE, k THE KERNEL SIZE, s THE STRIDE, p THE PADDING, AND f THE DROPOUT RATE. THE HIDDEN STATE SIZE CHANGES DEPENDING ON THE TIME SERIES LENGTH, AS DISCUSSED IN SECTION III-D.

	Layer (type)	Param #	Output Shape	Specifications
GRU	GRU (GRU)	9,984	(1, 32)	$h : 32$ or 64
	linear (Linear)	825	(1, 25)	
CNN	conv1† (Conv2D)	43,248	(1, 24, 15, 15)	$k : 15, s : 3, p : 2$
	conv2 (Conv2D)	115,296	(1, 48, 13, 13)	$k : 5, s : 1, p : 2$
	max_pool2d (MaxPool2D)		(1, 48, 7, 7)	$k : 2$
	dropout1 (Dropout2D)			$f : 0.25$
	fc1† (Linear)	1,410,456	(1, 408)	
	dropout2 (Dropout2D)			$f : 0.5$
FC Network	fc3† (Linear)	472	(1, 8)	
	fc4‡ (Linear)	36	(1, 4)	

Total parameters: 1,590,542

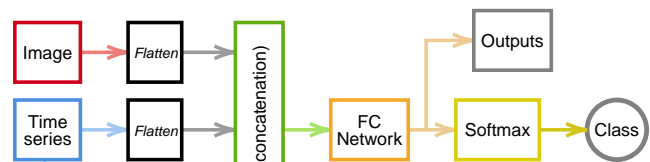


Fig. 3. **GloNet** architecture. The input data are (1) flattened, (2) concatenated, and (3) fed to a FC module.

LoNet, applies early fusion and relies on a Fully Connected sub-network applied to the flattened inputs. This approach is complementary to the one of LoNet: it combines the original time series and the original image up-front, rather than merging the features derived from their pre-processing by the GRU and CNN modules. Table III also shows that the number of parameters is higher than in LoNet. Having more parameters allows learning from more complex data, which compensates for the absence of convolutional layers.

TABLE III

GLO.NET ARCHITECTURE – THE † SYMBOL DENOTES THE USE OF RELU, WHILE THE ‡ SYMBOL INDICATES THE USE OF LOGSOFTMAX.

Layer (type)	Output Shape	Param #
fc1† (Linear)	(1, 1024)	8,332,288
fc2† (Linear)	(1, 256)	262,400
fc3† (Linear)	(1, 64)	16,448
fc4† (Linear)	(1, 8)	520
fc5‡ (Linear)	(1, 4)	36

Total parameters: 8,611,692

F. MuNet, a network focusing on local and global features

Figure 4 shows the architecture of the MuNet sub-network and Table IV summarizes its features. It processes the image using two parallel branches: a CNN and an FC sub-network. The time series is processed in the same way as in LoNet. Compared to LoNet, MuNet adds the FC module applied to the image, to extract local and global features simultaneously.

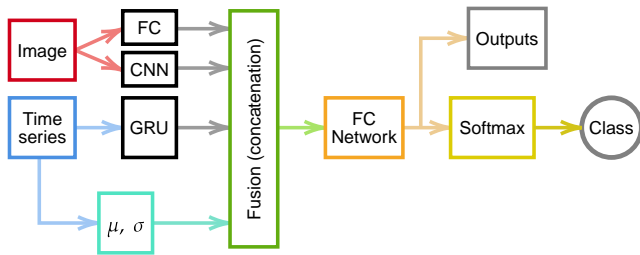


Fig. 4. **MuNet** architecture. While LoNet processes the image using only a CNN, MuNet employs both a (simpler) CNN and a FC component.

The latter may provide a relevant contribution due to the small size of the images. To avoid overfitting, the number of the CNN parameters is smaller than in LoNet and the number of parameters in the FC sub-network is smaller than in GloNet. In total, the number of parameters is similar to the one of GloNet.

TABLE IV

MUNET ARCHITECTURE – THE † SYMBOL DENOTES THE USE OF RELU, WHILE THE ‡ SYMBOL INDICATES THE USE OF LOGSOFTMAX. IN THE LAST COLUMN, h DENOTES THE SIZE OF THE GRU HIDDEN STATE, k THE KERNEL SIZE, s THE STRIDE, p THE PADDING, AND f THE DROPOUT RATE. THE HIDDEN STATE SIZE CHANGES DEPENDING ON THE TIME SERIES LENGTH, AS IN THE CASE OF LONET.

	Layer (type)	Param #	Output Shape	
FC	fc1 [†] (Linear)	8,295,424	(1, 1024)	
	fc2 [†] (Linear)	262,400	(1, 256)	
	fc3 [†] (Linear)	16,448	(1, 64)	
	fc4 (Linear)	1,625	(1, 25)	
GRU	GRU (GRU)	9,984	(1, 32)	$h : 32$ or 64
	linear (Linear)	825	(1, 25)	
CNN	conv1 [†] (Conv2D)	2,424	(1, 24, 15, 15)	$k : 5, s : 3, p : 2$
	conv2 (Conv2D)	28,848	(1, 48, 13, 13)	$k : 5, s : 1, p : 2$
	max_pool2d (MaxPool2D)		(1, 48, 7, 7)	$k : 2$
	dropout1 (Dropout2D)			$f : 0.25$
	fc1 [†] (Linear)	960,024	(1, 408)	
	dropout2 (Dropout2D)			$f : 0.5$
FC Network	fc5 [†] (Linear)	672	(1, 8)	
	fc6 [‡] (Linear)	36	(1, 4)	

Total parameters: 9,588,935

G. ReFuse

Figure 5 presents the ReFuse architecture and Table V summarizes its features. The inputs of ReFuse are the 12 outputs computed by LoNet, GloNet, and MuNet and the output is the predicted class. To avoid overfitting, the network is relatively shallow and contains only 154 parameters.

H. Training

The training process of DeepGraviLens is divided into two stages. In the first step, LoNet, GloNet, and MuNet are trained separately, using the same inputs. The best model for each sub-network is obtained as the one with the highest accuracy value on the validation set. The second stage consists of the training of the ReFuse sub-network, which exploits as inputs the values obtained before the application of the final activation function of the LoNet, GloNet, and MuNet sub-networks. LoNet, GloNet, and MuNet are trained for a maximum of 200

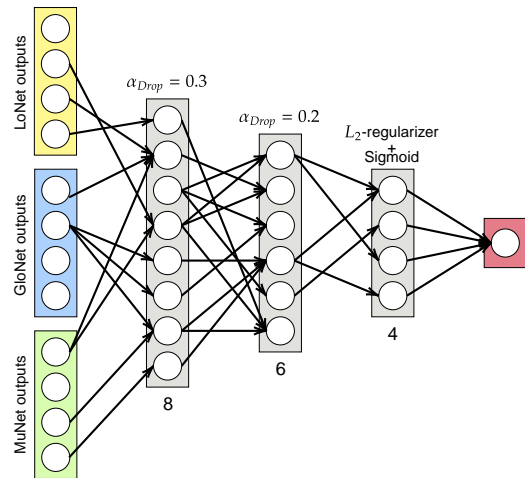


Fig. 5. **ReFuse** – The lack of connections between the hidden layers results from the use of dropout.

TABLE V

REFUSE ARCHITECTURE – REFUSE IS A FC NETWORK THAT CONTAINS 154 PARAMETERS. THE CHOSEN BATCH SIZE IS 512.

Layer (type)	Output Shape	Param #
dense (Dense)	(512, 8)	72
dropout (Dropout)	(512, 8)	
dense_1 (Dense)	(512, 6)	54
dropout_1 (Dropout)	(512, 6)	
dense_2 (Dense)	(512, 4)	28
activation (Activation)	(512, 4)	

Total parameters: 154

epochs, and the Early Stopping patience is set to 20 epochs. ReFuse, instead, is trained for 100 epochs. In both stages, the best model is the one with the highest validation accuracy.

IV. EVALUATION

This section reports the quantitative and qualitative evaluation of DeepGraviLens on the datasets introduced in III-A.

A. Quantitative results

This section presents the outcome of the performance analysis of DeepGraviLens on the four datasets described in Section III-A. For assessing the improvement induced by the proposed architecture, the approach of [41] is used as a baseline. Accuracy is used as the performance metric because the dataset is balanced. Ablation experiments with respect to the sub-networks preceding the final ReFuse stage are also performed to verify their contribution.

1) *Prediction performance*: Table VI presents the results on the train, validation and test sets. The test set accuracy is similar for the DESI-DOT, LSST-wide and DES-deep data sets and decreases for the more complex DES-wide data set. In all cases, the accuracy shows an improvement with respect to the baseline. The largest increment can be observed for the DES-wide dataset (+43.43%) and the smallest one for the LSST-wide dataset (+19.23%).

TABLE VI
ACCURACY – COMPARISON OF THE ACCURACY OF DEEPGRAVILENS AND OF THE BASELINE [41]. AN IMPROVEMENT OF $\approx 19\%$ TO $\approx 43\%$ IS ACHIEVED.

	Baseline	DeepGraviLens	Improvement
DES-deep	57.30%	99.12%	+41.82%
DES-wide	48.70%	92.13%	+43.43%
DESI-DOT	73.50%	98.36%	+24.86%
LSST-wide	78.50%	97.73%	+19.23%

Figure 6 shows the confusion matrices for the four data sets. For the DES-deep data set, the greatest confusion is observed between “No Lens” and “Lens”. A similar, yet more accentuated pattern, was found in [41] too.

For the DES-wide data set, the greatest confusion is between the LSN1a and LSNCC classes. This pattern is caused by the long interval between subsequent samples in the brightness time series, which hinders the ability to distinguish the short-lived explosion events that affect such systems. However, the combination of three fusion sub-networks reduces the confusion with respect to the baseline [41] significantly.

For the DESI-DOT data set, the test set accuracy is 98.39%, and the confusion between classes is lower than the one presented in [41]. The greatest confusion is between the “No Lens” and the “Lens” classes, which can be justified by the similarity of the brightness time series of some systems. An example is the “Galaxy + Star” system, in which a galaxy and a star appear close together but without the lensing effect, and the “Galaxy-Galaxy Lensing + Star” system, in which a galaxy stands in front of another galaxy producing the lensing effect and a star appears close to the lensed galaxy from the point of view of the observer.

For the LSST-wide data set the greatest confusion is between the “No Lens” and the “Lens” classes as in DESI-DOT because the time series in the two data sets have the same number of samples.

The reported results prove that DeepGraviLens can classify the samples of all the data sets accurately and with a significant performance improvement with respect to the baseline. DES-wide is the most challenging data set, as shown also in [41]. The reason is that lensed galaxies are fainter due to the simulated optical depth of the images, which depends on the technical characteristics of the simulated instrumentation. Moreover, the time series are shorter than in the other data sets and thus contain less information.

2) *Ablation studies*: Table VII presents the results of the ablation experiments with respect to the multi-modal data fusion sub-networks. For each data set, combining the three networks using ReFuse is better than combining two out of three networks or considering the output of a single network. In particular, Table VII shows that combining three networks yields an improvement ranging from +0.46% to +18.84% with respect to single networks, and an improvement ranging from +0.00% to +6.31% with respect to the combination of two networks.

In LSST-wide, the contribution of GloNet is dominated by

TABLE VII
ABLATION STUDIES – WHEN A SINGLE NETWORK IS CONSIDERED, ACCURACY REFERS TO THE RESULTS OBTAINED BY APPLYING IT WITHOUT REFUSE.

Data set	GloNet	LoNet	MuNet	Test accuracy
DES-deep	✓			94.35%
		✓		98.66%
			✓	95.89%
	✓	✓		97.58%
	✓		✓	92.81%
	✓	✓	✓	98.64%
DES-wide	✓			99.12%
		✓		88.98%
			✓	73.29%
	✓	✓		88.75%
	✓		✓	89.86%
	✓	✓	✓	90.39%
DESI-DOT	✓	✓	✓	89.31%
		✓		91.63%
			✓	97.55%
	✓	✓		93.54%
	✓		✓	98.21%
	✓	✓	✓	95.03%
LSST-wide	✓	✓	✓	98.08%
	✓	✓	✓	98.36%
	✓			90.77%
		✓		95.01%
	✓		✓	96.57%
	✓	✓	✓	95.86%
		✓	91.68%	
	✓	✓	97.73%	
	✓	✓	97.73%	

that of the other two sub-networks and thus eliminating GloNet does not affect accuracy. This can be explained by the use of early fusion in GloNet and by the fact that LSST-wide data series have low frequency and do not capture the fastest transient phenomena. In such cases, the image contains the useful information whereas the time series introduces noise, which makes the classification more challenging. Late fusion, instead, better preserves the information of the images.

The introduction of the means and standard deviations of the time series yields a modest average improvement of 0.86% of accuracy consistently across the data sets.

3) *Execution time*: DeepGraviLens has been trained using an NVIDIA GeForce GTX 1650 Ti GPU for GloNet and MuNet and an AMD Ryzen 7 4800H CPU for LoNet, which requires more memory. Table VIII summarizes the total training duration, in hours. On average, the network training requires less than 14 hours for a single data set. ReFuse training time is negligible with respect to the other networks. The duration is correlated with the data set complexity: DES-wide, which has the lowest quality data, requires almost 18 hours for training, while DESI-DOT, characterized by high-frequency time series, requires only 11 hours.

The inference time is independent of the data set. On average, inference requires 1.46 ms for a single input.

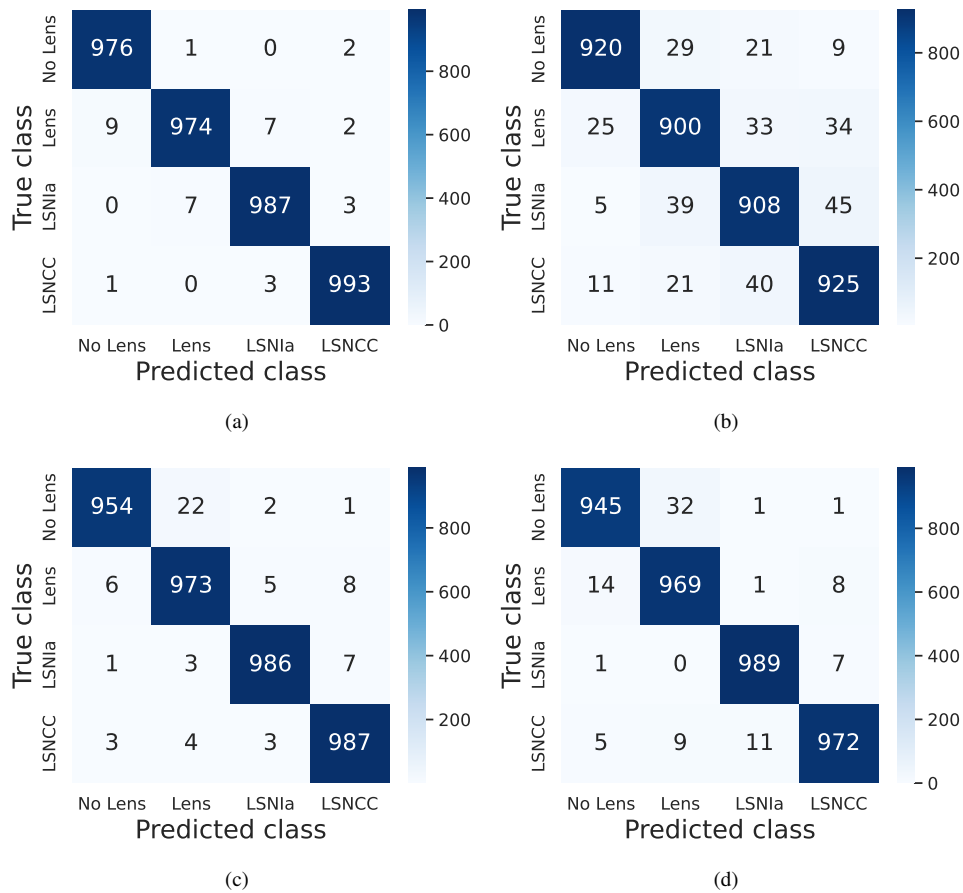


Fig. 6. **Confusion matrices** of the (a) DES-deep, (b) DES-wide, (c) DESI-DOT, and (d) LSST-wide data sets. In general, the greatest confusion is observed between “Lens” and “No Lens”, and in the case of the DES-wide data set, between “LSNCC” and “LSNiA”, due to the low sampling rate.

TABLE VIII

TRAINING TIME – THE TRAINING DURATION IS LESS THAN 14 HOURS PER DATA SET ON AVERAGE AND DEPENDS ON THE QUALITY OF THE DATA.

Data set	Training duration [h]				Total
	GloNet	LoNet	MuNet	ReFuse	
DES-deep	2.3	10.2	2.1	10^{-3}	14.6
DES-wide	2.6	12.0	3.3	10^{-3}	17.9
DESI-DOT	3.0	7.3	1.7	10^{-3}	11.0
LSST-wide	2.3	6.4	2.1	10^{-3}	10.8
					54.3

B. Qualitative results

This section illustrates some representative examples of the results obtained by DeepGraviLens on the four test sets. All the images are obtained by adding the *griz* layers, as done in [41]. In the plots, the *g* band is displayed in green, the *r* band in red, the *i* band in blue and the *z* band in grey.

Figure 7 presents a true positive example belonging to the “No Lens” class in the LSST-wide data set. It shows two stars close to each other, which present a spherical symmetry. Such symmetry suggests the absence of lensing. In addition, the brightness curves do not show consistent variations, which indicates the absence of transient phenomena.

Figure 8 presents a true positive example belonging to the “Lens” class, in the DESI-DOT data set. In this system, the lensing effect is manifested by the ring pattern on the central body. The flatness of the brightness curves indicates the absence of transient phenomena, as expected, because the system is formed by galaxies, which are not characterized by explosive events.

Figure 9 presents a true positive example belonging to the “LSNiA” class in the DESI-DOT data set. The peak in the time series indicates the presence of an exploding supernova and the image shows an elliptical shape, which signals the presence of lensing. The brightness in the *g* band is almost flat, which is distinctive of Type Ia supernovae. Type Ia and core-collapse supernovae release chemical elements during the explosion and produce photons at different wavelengths, which are detected by sensors in specific bands. During explosions, the emission of an element with a certain wavelength produces a temporary brightness peak in the corresponding band. Both types of supernovae release chemical elements whose detection can be observed in the *g* band, but Type-Ia supernovae emit less materials than core-collapse supernovae, which makes the latter exhibit a more pronounced peak in the *g* band. The absence of such a peak in Figure 9 justifies the “LSNiA” classification.

The same type of system is shown in Figure 10, from the

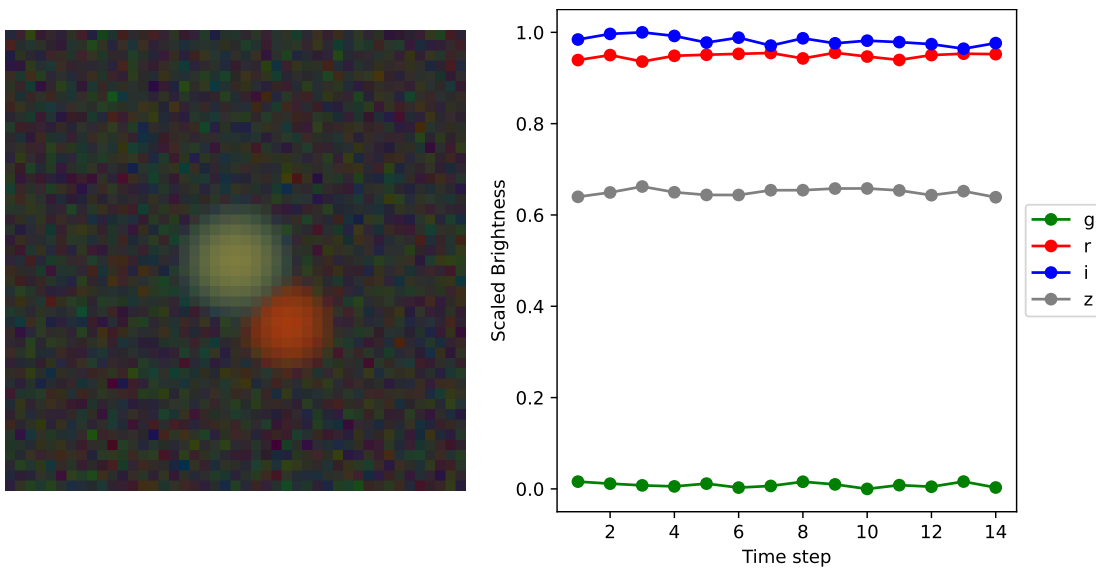


Fig. 7. A positive example on the LSST-wide data set – This datum belongs to the “No Lens” class. The image shows two separate stars that have a spherical geometry, which suggests they are not lensed. Moreover, the curves on the right show no consistent brightness variation through time, which indicates the absence of transient phenomena.

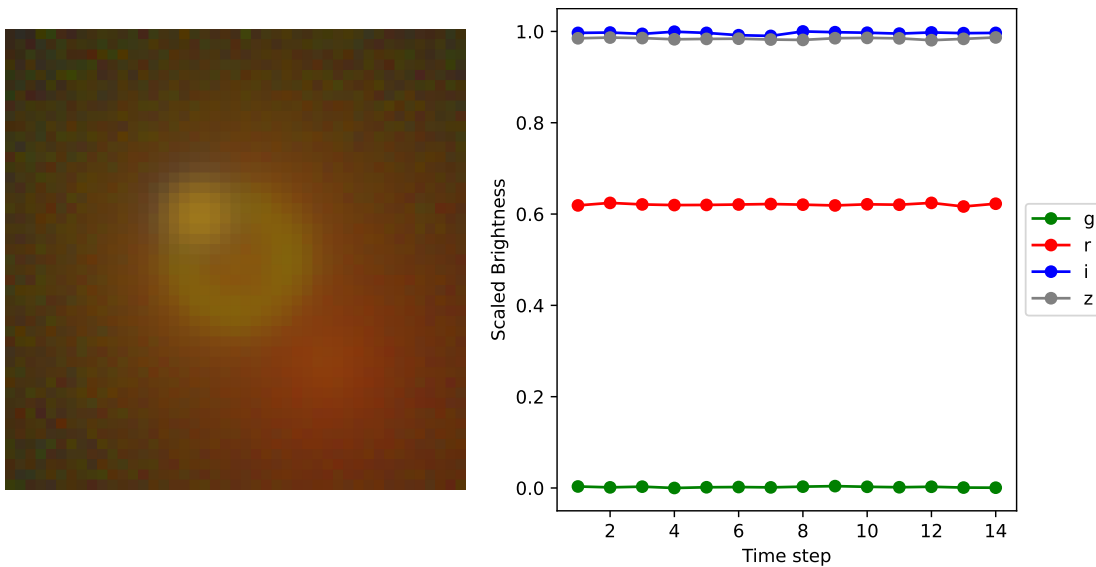


Fig. 8. A positive example on the DESI-DOT data set – This datum belongs to the “Lens” class. The lensing effect is visible in the ring pattern around the central body. The flatness of the brightness time series, instead, indicates the absence of transient phenomena (e.g., explosions), which is expected because the involved entities are galaxies.

DES-wide data set. In this case, the peaks are not detected because of the lower sampling rate, which misses rapid transient events. However, the network correctly classifies this example thanks to the information contained in the image.

Figure 11 presents a true positive example belonging to the “LSNCC” class, in the DESI-DOT data set. In this case, the presence of a supernova is indicated by the rapid variation in the brightness time series. Since also the g band exhibits a peak, the input is classified as a core-collapse supernova. The lensing effect is manifested in the image by the supernova (the green body), lensed by the galaxy in front of it. The green color confirms the presence of elements emitting photons in the g band and the body itself is visible because of the magnifying

effect induced by the galaxy.

Figure 12 presents a negative example in the LSST-wide data set. The datum belongs to the “LSNCC” class, but is classified as “Lens”, which means that the model was not able to detect the presence of a supernova and interpreted the example as a “galaxy-galaxy system”. The wrong classification is caused by the low-quality time series and the ambiguous image. The lensing effect is visible thanks to the faint halo surrounding the star in the background, but the time series (wrongly) suggest the absence of a transient phenomenon. The apparent lack of the transient phenomenon can be explained by considering that supernovae explosions can happen in a short time and the brightness variation may not be recorded by the

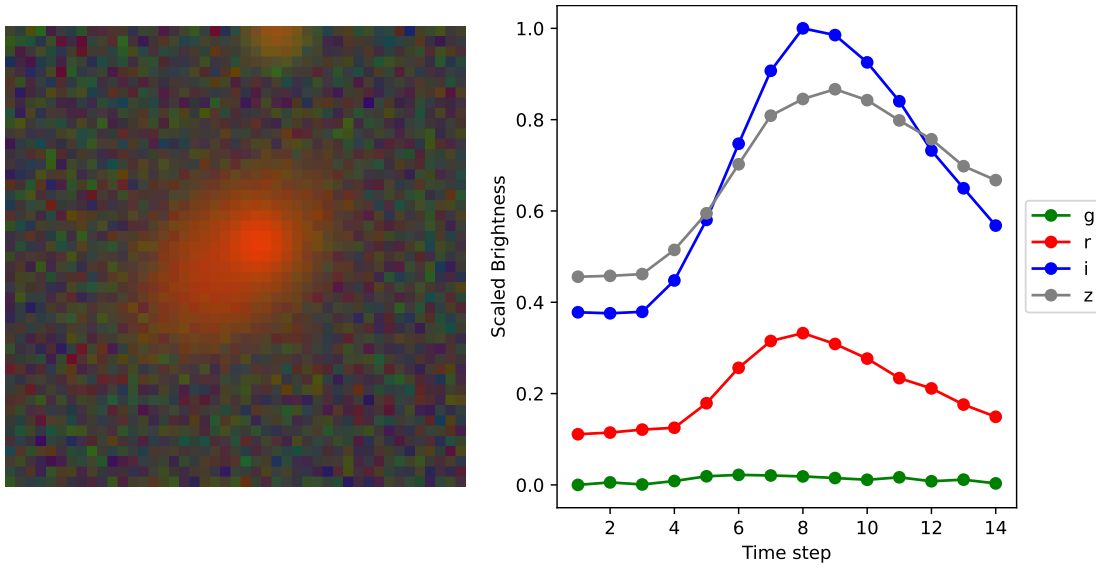


Fig. 9. A positive example on the DESI-DOT data set – This datum belongs to the “LSNIa” class. The lensing effect is visible from the elliptical shape of the central body, while the presence of a supernova can be observed by the peaks in the brightness time series, which indicates the presence of explosive transient phenomena. The supernova type can be inferred from the flatness of the g band time series.

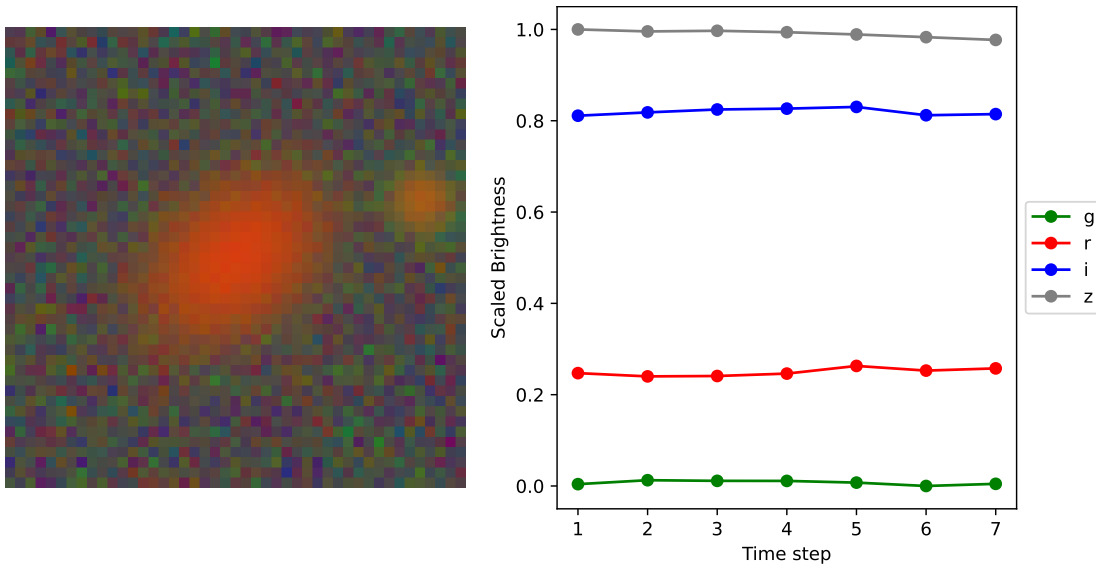


Fig. 10. A positive example on the DES-wide data set – This datum belongs to the “LSNIa” class. The lensing effect is visible because of the elliptical shape of the central body. Even if the peaks that indicate the presence of transient phenomena are absent, the network is still able to correctly classify the datum.

camera. Soon after the explosion, the brightness returns to the original value, which explains the flatness of the curves.

Figure 13 presents a negative example on the DES-deep data set, belonging to the “Lens” class, but classified as “No Lens”. The lensing effect is visible on the central body, which has a ring-like halo. However, because of the low image resolution, this effect is not as clear in most of the positive examples. In addition, the presence of multiple peaks is not frequently associated with the “Lens” class and induces the wrong classification. The same system simulated in the DESI-DOT data set (Figure 14) is classified correctly. The same ring pattern is visible, but the time series are consistent with the expected ones. The difference is likely caused by the shorter

time series of the DESI-DOT data set, which do not record long-duration phenomena such as a transiting star.

As a final example, Figure 15 shows an ambiguous image in the DESI-DOT data set, incorrectly classified. The sample belongs to the “No Lens” class, but is classified as “Lens”. The confusion is generated chiefly by the similarity in the colors of the objects visible in the image. Their elliptical shape is barely recognizable and has been confused for a lensing effect, while it can represent, e.g., a non-lensed elliptical galaxy. The time series are flat, so they do not help discern “Lens” and “No Lens” systems, because some “No Lens” systems also have flat time series.

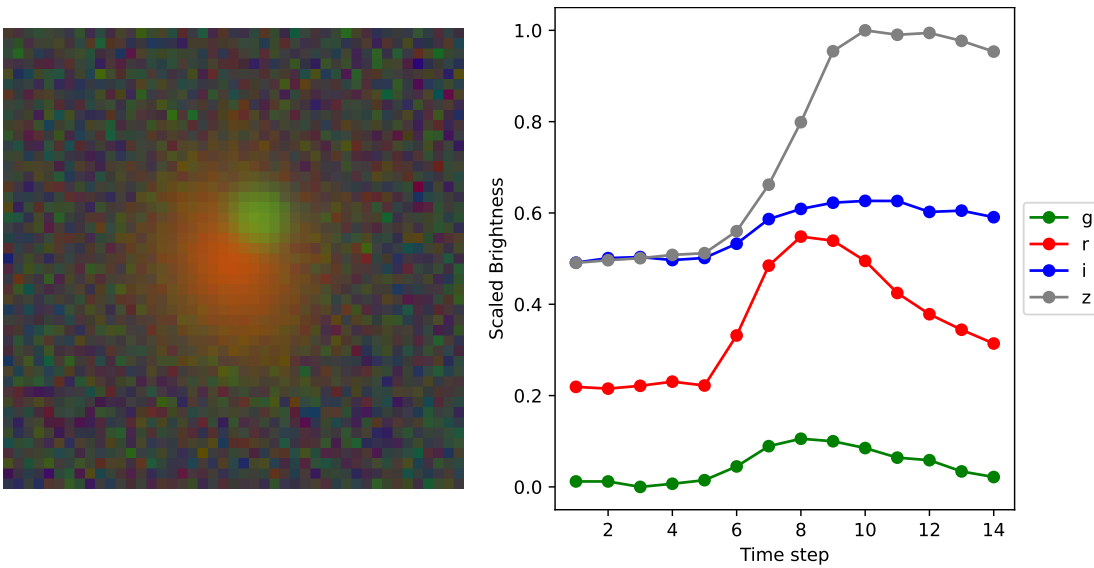


Fig. 11. A positive example on the DESI-DOT data set – This datum belongs to the “LSNCC” class. In this case, the lensing effect is suggested both by the presence of varying time curves (indicating the presence of a supernova) and the green body lensed by the galaxy.

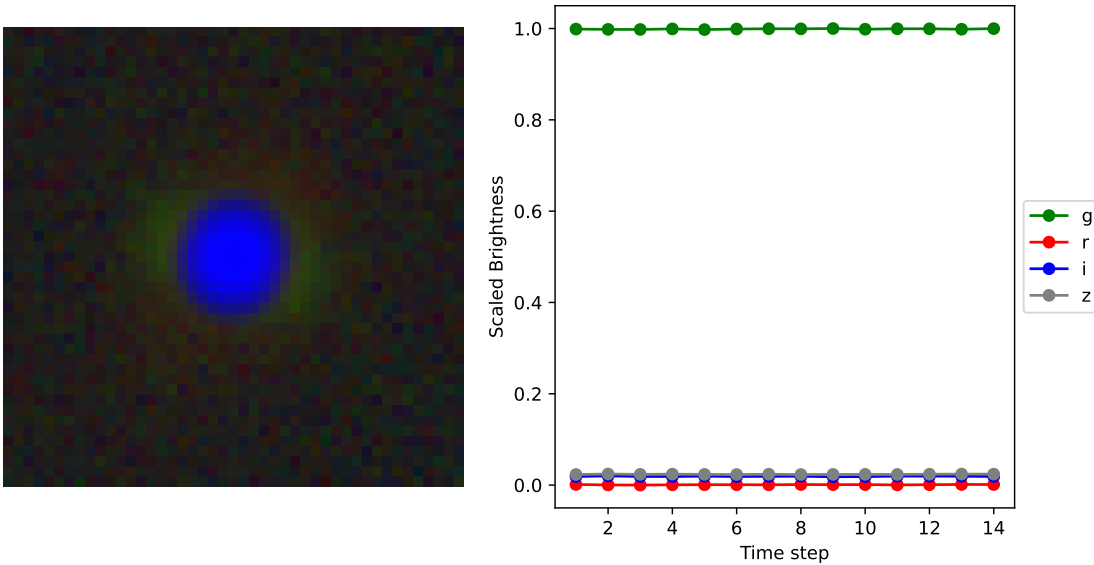


Fig. 12. A negative example on the LSST-wide data set – This datum belongs to the “LSNCC” class, but has been classified as “Lens”. The lensing effect is alluded by the halo surrounding the star, while the flat time series suggests the absence of a transient phenomenon, which induces the wrong classification.

V. CONCLUSIONS AND FUTURE WORK

This work has introduced DeepGraviLens, a deep neural architecture for the classification of simulated gravitational lensing phenomena that processes multi-modal inputs by means of sub-networks focusing on complementary data aspects. DeepGraviLens surpasses the state-of-the-art accuracy results by a large margin, with increments ranging from $\approx 19\%$ to $\approx 43\%$ on four simulated data sets with different data quality. In particular, it attains a 19.23% performance increase on the LSST-wide data set, which simulates the acquisitions of the Vera C. Rubin Observatory whose operations are scheduled to start in 2023. The Vera C. Rubin Observatory is expected to detect hundreds to thousands of lensed supernovae systems, which represents a break-through with respect to the capacity of previous instruments. The enormous amount of data that

will be acquired demands highly accurate and fast computer-aided classification tools, such as DeepGraviLens.

Future work will concentrate on the application of DeepGraviLens to real observations as soon as they become available. The envisioned research work will also pursue the objective of creating a scientist-friendly system that allows experts to import and manually classify data from real observations to create a non-simulated data set and compute relevant classification and object detection metrics for automated data analysis, following an approach similar to the one implemented in [62], [63], [74]. Finally, we plan to employ the multi-modal architecture designed for DeepGraviLens for the analysis of other (possibly non-astrophysical) data sets characterized by images and time series.

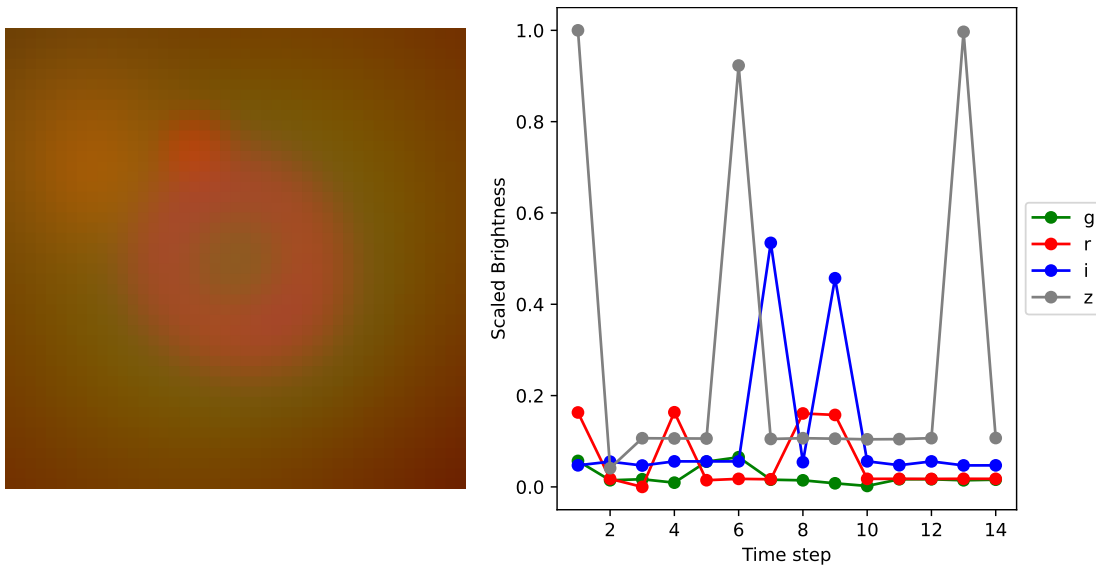


Fig. 13. A negative example on the DES-deep data set – This datum belongs to the “Lens” class, but has been classified as “No Lens”. The lensing effect is suggested by the ring surrounding the central body.

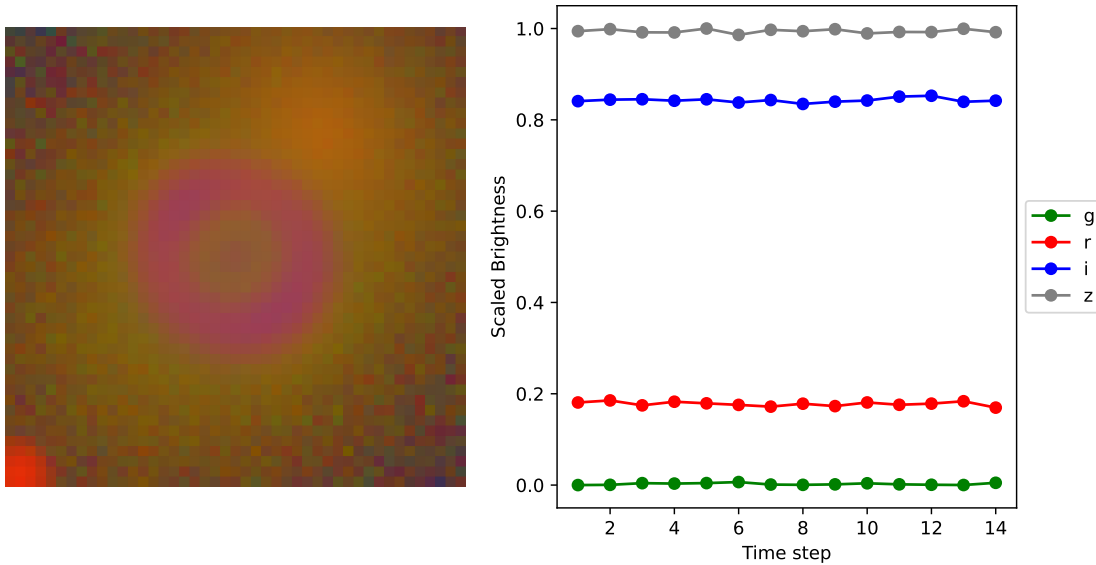


Fig. 14. A positive example on the DESI-DOT data set – This datum belongs to the “Lens” class, and represents the same system shown in Figure 13. In this case, the lensing effect is indicated by the ring around the central body and the type of lensing by the flat time series.

ACKNOWLEDGMENT

The authors thank Robert Morgan, author of [41], for having provided guidance in the use of the `deeplens` simulator and the generation and use of the data set, and professors Hans Georg Schaathun and Ben David Normann for proofreading the article.

REFERENCES

- [1] T. M. C. Abbott, F. B. Abdalla, S. Allam, A. Amara, J. Annis, J. Asorey, S. Avila, O. Ballester, M. Banerji, W. Barkhouse, L. Baruah, M. Baumer, K. Bechtol, M. R. Becker, A. Benoit-Lévy, G. M. Bernstein, E. Bertin, J. Blazek, S. Bocquet, D. Brooks, D. Brout, E. Buckley-Geer, D. L. Burke, V. Busti, R. Campisano, L. Cardiel-Sas, A. Carnero Rosell, M. Carrasco Kind, J. Carretero, F. J. Castander, R. Cawthon, C. Chang, X. Chen, C. Conselice, G. Costa, M. Crocce, C. E. Cunha, C. B. D’Andrea, L. N. da Costa, R. Das, G. Daues, T. M. Davis, C. Davis,

- J. De Vicente, D. L. DePoy, J. DeRose, S. Desai, H. T. Diehl, J. P. Dietrich, S. Dodelson, P. Doel, A. Drlica-Wagner, T. F. Eifler, A. E. Elliott, A. E. Evrard, A. Farahi, A. Fausti Neto, E. Fernandez, D. A. Finley, B. Flaugher, R. J. Foley, P. Fosalba, D. N. Friedel, J. Frieman, J. García-Bellido, E. Gaztanaga, D. W. Gerdes, T. Giannantonio, M. S. S. Gill, K. Glazebrook, D. A. Goldstein, M. Gower, D. Gruen, R. A. Gruendl, J. Gschwend, R. R. Gupta, G. Gutierrez, S. Hamilton, W. G. Hartley, S. R. Hinton, J. M. Hislop, D. Hollowood, K. Honscheid, B. Hoyle, D. Huterer, B. Jain, D. J. James, T. Jeltema, M. W. G. Johnson, M. D. Johnson, T. Kacprzak, S. Kent, G. Khullar, M. Klein, A. Kovacs, A. M. G. Koziol, E. Krause, A. Kremin, R. Kron, K. Kuehn, S. Kuhlmann, N. Kuropatkin, O. Lahav, J. Lasker, T. S. Li, R. T. Li, A. R. Liddle, M. Lima, H. Lin, P. López-Reyes, N. MacCrann, M. A. G. Maia, J. D. Maloney, M. Manera, M. March, J. Marriner, J. L. Marshall, P. Martini, T. McClintock, T. McKay, R. G. McMahon, P. Melchior, F. Menanteau, C. J. Miller, R. Miquel, J. J. Mohr, E. Morganson, J. Mould, E. Neilsen, R. C. Nichol, F. Nogueira, B. Nord, P. Nugent, L. Nunes, R. L. C. Ogando, L. Old, A. B. Pace, A. Palmese, F. Paz-Chinchón, H. V. Peiris, W. J. Percival, D. Petravick, A. A. Plazas, J. Poh, C. Pond, A. Porredon, A. Pujol, A. Refregier, K. Reil, P. M. Ricker,

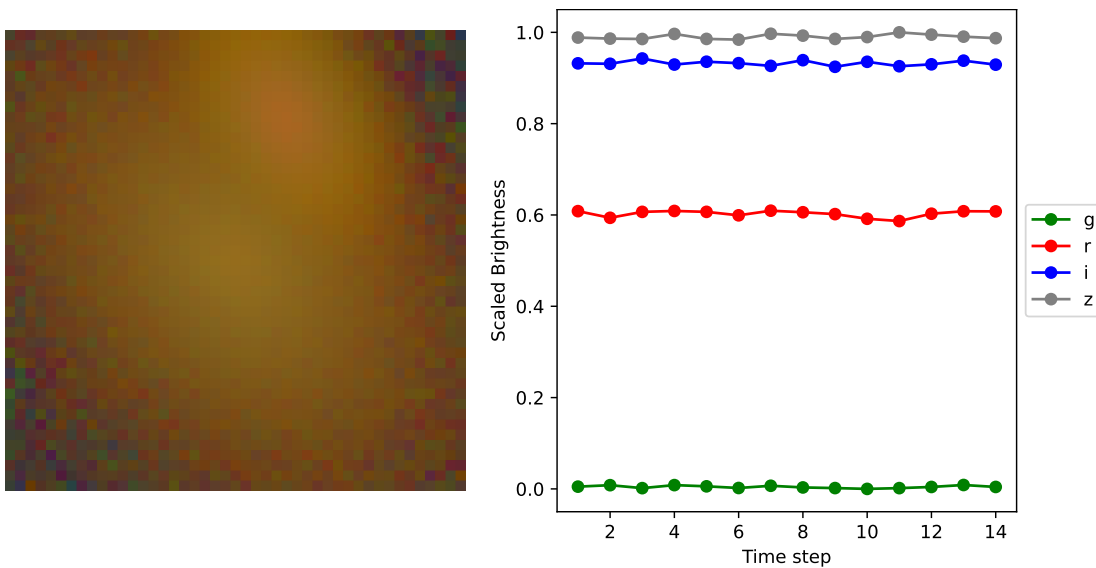


Fig. 15. **A negative example on the DESI-DOT data set** – This datum belongs to the “No Lens” class, but it has been classified as belonging to the “Lens” class. In this example, it is difficult to understand which objects are contained in the image, as their colors are similar. The lensing effect is suggested by the elliptical shape, but such shape may suggest also the presence of a non-lensing elliptical galaxy. The flatness of the time series, in addition, does not allow to discern “Lens” and “No Lens” systems, as some “No Lens” systems also have flat time series.

- R. P. Rollins, A. K. Romer, A. Roodman, P. Rooney, A. J. Ross, E. S. Rykoff, M. Sako, M. L. Sanchez, E. Sanchez, B. Santiago, A. Saro, V. Scarpine, D. Scolnic, S. Serrano, I. Sevilla-Noarbe, E. Sheldon, N. Shipp, M. L. Silveira, M. Smith, R. C. Smith, J. A. Smith, M. Soares-Santos, F. Sobreira, J. Song, A. Stebbins, E. Suchyta, M. Sullivan, M. E. C. Swann, G. Tarle, J. Thaler, D. Thomas, R. C. Thomas, M. A. Troxel, D. L. Tucker, V. Vikram, A. K. Vivas, A. R. Walker, R. H. Wechsler, J. Weller, W. Wester, R. C. Wolf, H. Wu, B. Yanny, A. Zenteno, Y. Zhang, J. Zuntz, S. Juneau, M. Fitzpatrick, R. Nikutta, D. Nidever, K. Olsen, A. Scott, and and. The dark energy survey: Data release 1. *The Astrophysical Journal Supplement Series*, 239(2):18, nov 2018.
- [2] T. M. C. Abbott, S. Allam, P. Andersen, C. Angus, J. Asorey, A. Avelino, S. Avila, B. A. Bassett, K. Bechtol, G. M. Bernstein, E. Bertin, D. Brooks, D. Brout, P. Brown, D. L. Burke, J. Calcino, R. Carnero Rosell, D. Carollo, M. Carrasco Kind, J. Carretero, R. Casas, F. J. Castander, R. Cawthon, P. Challis, M. Childress, A. Clocchiatti, C. E. Cunha, C. B. D’Andrea, L. N. da Costa, C. Davis, T. M. Davis, J. De Vicente, D. L. DePoy, S. Desai, H. T. Diehl, P. Doel, A. Drlica-Wagner, T. F. Eifler, A. E. Evrard, E. Fernandez, A. V. Filippenko, D. A. Finley, B. Flaugher, R. J. Foley, P. Fosalba, J. Frieman, L. Galbany, J. Garcia-Bellido, E. Gaztanaga, T. Giannantonio, K. Glazebrook, D. A. Goldstein, S. González-Gaitán, D. Gruen, R. A. Gruendl, J. Gschwend, R. G. Gupta, G. Gutierrez, W. G. Hartley, S. R. Hinton, D. L. Hollowood, K. Honscheid, J. K. Hoormann, B. Hoyle, D. J. James, T. Jeltema, M. W. G. Johnson, M. D. Johnson, E. Kasai, S. Kent, R. Kessler, A. G. Kim, R. P. Kirshner, E. Kovacs, E. Krause, R. Kron, K. Kuehn, S. Kuhlmann, N. Kuropatkin, O. Lahav, J. Lasker, G. F. Lewis, T. S. Li, C. Lidman, M. Lima, H. Lin, E. Macaulay, M. A. G. Maia, K. S. Mandel, M. March, J. Marriner, J. L. Marshall, P. Martini, F. Menanteau, C. J. Miller, R. Miquel, V. Miranda, J. J. Mohr, E. Morganson, D. Muthukrishna, A. Möller, E. Neilsen, R. C. Nichol, B. Nord, P. Nugent, R. L. C. Ogando, A. Palmese, Y.-C. Pan, A. A. Plazas, M. Pursiainen, A. K. Romer, A. Roodman, E. Roza, E. S. Rykoff, M. Sako, E. Sanchez, V. Scarpine, R. Schindler, M. Schubnell, D. Scolnic, S. Serrano, I. Sevilla-Noarbe, R. Sharp, M. Smith, M. Soares-Santos, F. Sobreira, N. E. Sommer, H. Spinka, E. Suchyta, M. Sullivan, E. Swann, G. Tarle, D. Thomas, R. C. Thomas, M. A. Troxel, B. E. Tucker, S. A. Uddin, A. R. Walker, W. Wester, P. Wiseman, R. C. Wolf, B. Yanny, B. Zhang, and Y. Zhang and. First cosmology results using type Ia supernovae from the Dark Energy Survey: Constraints on cosmological parameters. *The Astrophysical Journal*, 872(2):L30, feb 2019.
- [3] Pablo Azagra, Yoan Mollard, Florian Golemo, Ana Cristina Murillo, Manuel Lopes, and Javier Civera. A multimodal human-robot interaction dataset. In *NIPS 2016, workshop Future of Interactive Learning Machines*, 2016.
- [4] Oresti Banos, Claudia Villalonga, Rafael Garcia, Alejandro Saez, Miguel Damas, Juan A. Holgado-Terriza, Sungyong Lee, Hector Pomares, and Ignacio Rojas. Design, implementation and validation of a novel open framework for agile development of mobile health applications. *Biomedical engineering online*, 14(2):1–20, 2015.
- [5] Simon Birrer, Anowar J Shajib, Daniel Gilman, Aymeric Galan, Jelle Aalbers, Martin Millon, Robert Morgan, Giulia Pagano, Ji Won Park, Luca Teodori, et al. lenstronomy ii: A gravitational lensing software ecosystem. *arXiv preprint arXiv:2106.05976*, 2021.
- [6] Yu Cao, Shawn Steffey, Jianbiao He, Degui Xiao, Cui Tao, Ping Chen, and Henning Müller. Medical image retrieval: a multimodal approach. *Cancer informatics*, 13:CIN-S14053, 2014.
- [7] Kyunghyun Cho, Bart Van Merriënboer, Caglar Gulcehre, Dzmitry Bahdanau, Fethi Bougares, Holger Schwenk, and Yoshua Bengio. Learning phrase representations using rnn encoder-decoder for statistical machine translation. *arXiv preprint arXiv:1406.1078*, 2014.
- [8] Junyoung Chung, Caglar Gulcehre, KyungHyun Cho, and Yoshua Bengio. Empirical evaluation of gated recurrent neural networks on sequence modeling. *arXiv preprint arXiv:1412.3555*, 2014.
- [9] Yucel Cimtay, Erhan Ekmekcioglu, and Seyma Caglar-Ozhan. Cross-subject multimodal emotion recognition based on hybrid fusion. *IEEE Access*, 8:168865–168878, 2020.
- [10] Jasmine Collins, Jascha Sohl-Dickstein, and David Sussillo. Capacity and trainability in recurrent neural networks. *arXiv preprint arXiv:1611.09913*, 2016.
- [11] Håkon Dahle, Nick Kaiser, Ragnvald J Irgens, Per B Lilje, and Steve J Maddox. Weak gravitational lensing by a sample of X-ray luminous clusters of galaxies. I. the data set. *The Astrophysical Journal Supplement Series*, 139(2):313, 2002.
- [12] Andrew Davies, Stephen Serjeant, and Jane M Bromley. Using convolutional neural networks to identify gravitational lenses in astronomical images. *Monthly Notices of the Royal Astronomical Society*, 487(4):5263–5271, 05 2019.
- [13] H. T. Diehl, E. Neilsen, R. A. Gruendl, T. M. C. Abbott, S. Allam, O. Alvarez, J. Annis, E. Balbinot, S. Bhargava, K. Bechtol, G. M. Bernstein, R. Bhatawdekar, S. Bocquet, D. Brout, R. Capasso, R. Cawthon, C. Chang, E. Cook, C. J. Conselice, J. Cruz, C. D’Andrea, L. da Costa, R. Das, D. L. DePoy, A. Drlica-Wagner, A. Elliott, S. W. Everett, J. Frieman, A. Fausti Neto, A. Ferté, I. Friswell, K. E. Furnell, L. Gelman, D. W. Gerdes, M. S. S. Gill, D. A. Goldstein, D. Gruen, D. J. Gullledge, S. Hamilton, D. Hollowood, K. Honscheid, D. J. James, M. D. Johnson, M. W. G. Johnson, S. Kent, R. S. Kessler, G. Khullar, E. Kovacs, A. Kremin, R. Kron, N. Kuropatkin, J. Lasker, A. Lathrop, T. S. Li, M. Manera, M. March, J. L. Marshall, M. Medford, F. Menanteau, I. Mohammed, M. Monroy, B. Moraes, E. Morganson, J. Muir, M. Murphy, B. Nord, A. B. Pace, A. Palmese, Y. Park, F. Paz-Chinchón,

- M. E. S. Pereira, D. Petravick, A. A. Plazas, J. Poh, T. Prochaska, A. K. Romer, K. Reil, A. Roodman, M. Sako, M. Sauseda, D. Scolnic, L. F. Secco, I. Sevilla-Noarbe, N. Shipp, J. A. Smith, M. Soares-Santos, B. Soergel, A. Stebbins, K. T. Story, K. Stringer, F. Tarsitano, B. Thomas, D. L. Tucker, K. Vivas, A. R. Walker, M.-Y. Wang, C. Weaverdyck, N. Weaverdyck, W. Wester, C. F. Wethers, R. Wilkenson, H.-Y. Wu, B. Yanny, A. Zenteno, and Y. Zhang. Dark energy survey operations: years 4 and 5. In Alison B. Peck, Robert L. Seaman, and Chris R. Benn, editors, *Observatory Operations: Strategies, Processes, and Systems VII*, volume 10704, pages 138 – 155. International Society for Optics and Photonics, SPIE, 2018.
- [14] Isaac Elias, Heiga Zen, Jonathan Shen, Yu Zhang, Ye Jia, Ron J Weiss, and Yonghui Wu. Parallel tacotron: Non-autoregressive and controllable tts. In *ICASSP 2021-2021 IEEE International Conference on Acoustics, Speech and Signal Processing (ICASSP)*, pages 5709–5713. IEEE, 2021.
- [15] Ridi Ferdiana, William Fajar Dicka, and Alfred Boediman. Cat sounds classification with convolutional neural network. *International Journal on Electrical Engineering and Informatics*, 13(3):755–765, 2021.
- [16] B. Flaughner, H. T. Diehl, K. Honscheid, T. M. C. Abbott, O. Alvarez, R. Angstadt, J. T. Annis, M. Antonik, O. Ballester, L. Beaufore, G. M. Bernstein, R. A. Bernstein, B. Bigelow, M. Bonati, D. Boprie, D. Brooks, E. J. Buckley-Geer, J. Campa, L. Cardiel-Sas, F. J. Castander, J. Castilla, H. Cease, J. M. Cela-Ruiz, S. Chappa, E. Chi, C. Cooper, L. N. da Costa, E. Dede, G. Derylo, D. L. DePoy, J. de Vicente, P. Doel, A. Drlca-Wagner, J. Eiting, A. E. Elliott, J. Emes, J. Estrada, A. Fausti Neto, D. A. Finley, R. Flores, J. Frieman, D. Gerdes, M. D. Gladders, B. Gregory, G. R. Gutierrez, J. Hao, S. E. Holland, S. Holm, D. Huffman, C. Jackson, D. J. James, M. Jonas, A. Karcher, I. Karliner, S. Kent, R. Kessler, M. Kozlovsky, R. G. Kron, D. Kubik, K. Kuehn, S. Kuhlmann, K. Kuk, O. Lahav, A. Lathrop, J. Lee, M. E. Levi, P. Lewis, T. S. Li, I. Mandrichenko, J. L. Marshall, G. Martinez, K. W. Merritt, R. Miquel, F. Muñoz, E. H. Neilsen, R. C. Nichol, B. Nord, R. Ogando, J. Olsen, N. Palaio, K. Patton, J. Peoples, A. A. Plazas, J. Rauch, K. Reil, J.-P. Rheault, N. A. Roe, H. Rogers, A. Roodman, E. Sanchez, V. Scarpine, R. H. Schindler, R. Schmidt, R. Schmitt, M. Schubnell, K. Schultz, P. Schurter, L. Scott, S. Serrano, T. M. Shaw, R. C. Smith, M. Soares-Santos, A. Stefanik, W. Stuermer, E. Suchyta, A. Sypniewski, G. Tarle, J. Thaler, R. Tighe, C. Tran, D. Tucker, A. R. Walker, G. Wang, M. Watson, C. Weaverdyck, W. Wester, R. Woods, and B. Yanny and. THE DARK ENERGY CAMERA. *The Astronomical Journal*, 150(5):150, oct 2015.
- [17] Jing Gao, Peng Li, Zhikui Chen, and Jianing Zhang. A survey on deep learning for multimodal data fusion. *Neural Computation*, 32(5):829–864, 2020.
- [18] Andreas Geiger, Philip Lenz, Christoph Stiller, and Raquel Urtasun. Vision meets robotics: The kitti dataset. *The International Journal of Robotics Research*, 32(11):1231–1237, 2013.
- [19] Daniel Gibert, Carles Mateu, and Jordi Planes. HYDRA: A multimodal deep learning framework for malware classification. *Computers & Security*, 95:101873, 2020.
- [20] Daniel A Goldstein and Peter E Nugent. How to find gravitationally lensed type Ia supernovae. *The Astrophysical Journal Letters*, 834(1):L5, 2016.
- [21] MV Gorenstein, II Shapiro, NL Cohen, BE Corey, EE Falco, JM Marcaide, AEE Rogers, AR Whitney, RW Porcas, RA Preston, et al. Detection of a compact radio source near the center of a gravitational lens: quasar image or galactic core? *Science*, 219(4580):54–56, 1983.
- [22] P. Hartley, R. Flamarly, N. Jackson, A. S. Tagore, and R. B. Metcalf. Support vector machine classification of strong gravitational lenses. *Monthly Notices of the Royal Astronomical Society*, 471(3):3378–3397, 07 2017.
- [23] Devamanyu Hazarika, Soujanya Poria, Rada Mihalcea, Erik Cambria, and Roger Zimmermann. Icon: Interactive conversational memory network for multimodal emotion detection. In *Proceedings of the 2018 conference on empirical methods in natural language processing*, pages 2594–2604, 2018.
- [24] Sepp Hochreiter and Jürgen Schmidhuber. Long short-term memory. *Neural computation*, 9(8):1735–1780, 1997.
- [25] Yongrui Huang, Jianhao Yang, Pengkai Liao, and Jiahui Pan. Fusion of facial expressions and EEG for multimodal emotion recognition. *Computational intelligence and neuroscience*, 2017, 2017.
- [26] Shafqat Ul Islam, Jitendra Kumar, and Sushant G Ghosh. Strong gravitational lensing by rotating Simpson-Visser black holes. *Journal of Cosmology and Astroparticle Physics*, 2021(10):013, 2021.
- [27] Željko Ivezić, Steven M Kahn, J Anthony Tyson, Bob Abel, Emily Acosta, Robyn Allsman, David Alonso, Yusra AlSayyad, Scott F Anderson, John Andrew, et al. LSST: from science drivers to reference design and anticipated data products. *The Astrophysical Journal*, 873(2):111, 2019.
- [28] Mimansa Jaiswal, Zakaria Aldeneh, and Emily Mower Provost. Controlling for confounders in multimodal emotion classification via adversarial learning. In *2019 International Conference on Multimodal Interaction*, pages 174–184, 2019.
- [29] Xing-Hua Jin, Yuan-Xing Gao, and Dao-Jun Liu. Strong gravitational lensing of a 4-dimensional Einstein–Gauss–Bonnet black hole in homogeneous plasma. *International Journal of Modern Physics D*, 29(09):2050065, 2020.
- [30] Rafal Jozefowicz, Wojciech Zaremba, and Ilya Sutskever. An empirical exploration of recurrent network architectures. In *International conference on machine learning*, pages 2342–2350. PMLR, 2015.
- [31] CR Lawrence, DP Schneider, M Schmidt, CL Bennett, JN Hewitt, BF Burke, EL Turner, and JE Gunn. Discovery of a new gravitational lens system. *Science*, 223(4631):46–49, 1984.
- [32] Minjia Li, Lun Xie, Zeping Lv, Juan Li, and Zhiliang Wang. Multistep deep system for multimodal emotion detection with invalid data in the internet of things. *IEEE Access*, 8:187208–187221, 2020.
- [33] Muxuan Liang, Zhizhong Li, Ting Chen, and Jianyang Zeng. Integrative data analysis of multi-platform cancer data with a multimodal deep learning approach. *IEEE/ACM transactions on computational biology and bioinformatics*, 12(4):928–937, 2014.
- [34] Hyun-il Lim. A study on dropout techniques to reduce overfitting in deep neural networks. In *Advanced Multimedia and Ubiquitous Engineering*, pages 133–139. Springer, 2021.
- [35] Maofu Liu, Huijun Hu, Lingjun Li, Yan Yu, and Weili Guan. Chinese image caption generation via visual attention and topic modeling. *IEEE transactions on cybernetics*, 2020.
- [36] Maofu Liu, Lingjun Li, Huijun Hu, Weili Guan, and Jing Tian. Image caption generation with dual attention mechanism. *Information Processing & Management*, 57(2):102178, 2020.
- [37] Sheng Liu, Zhou Ren, and Junsong Yuan. Sibnet: Sibling convolutional encoder for video captioning. *IEEE transactions on pattern analysis and machine intelligence*, 43(9):3259–3272, 2020.
- [38] Will Maddern, Geoffrey Pascoe, Chris Linegar, and Paul Newman. 1 year, 1000 km: The Oxford RobotCar dataset. *The International Journal of Robotics Research*, 36(1):3–15, 2017.
- [39] Phil Marshall, Will Clarkson, Ohad Shemmer, Rahul Biswas, Miguel de Val-Borro, Jeonghee Rho, Lynne Jones, Timo Anguita, Stephen Ridgway, Federica Bianco, Zeljko Ivezić, Michelle Lochner, Josh Meyers, Kathy Vivas, Melissa Graham, Chuck Claver, Seth Digel, Vishal Kasliwal, Peregrine M McGehee, Eric Gawiser, Eric Bellm, Lucianne Walkowicz, Knut Olsen, Peter Yoachim, Keaton Bell, David Nidever, Michael Lund, Andrew Connolly, Iair Arcavi, and Humna Awan. LSST Science Collaborations Observing Strategy White Paper: “Science-driven Optimization of the LSST Observing Strategy”, August 2017.
- [40] Philip J Marshall, David W Hogg, Leonidas A Moustakas, Christopher D Fassnacht, Maruša Bradač, Tim Schrabback, and Roger D Blandford. Automated detection of galaxy-scale gravitational lenses in high-resolution imaging data. *The Astrophysical Journal*, 694(2):924, 2009.
- [41] Robert Morgan, Brian Nord, Keith Bechtol, SJ González, E Buckley-Geer, A Möller, JW Park, AG Kim, S Birrer, M Agüena, et al. DeepZipper: A novel deep-learning architecture for lensed supernovae identification. *The Astrophysical Journal*, 927(1):109, 2022.
- [42] Robert Morgan, Brian Nord, Simon Birrer, Joshua Yao-Yu Lin, and Jason Poh. deepLenstronomy: A dataset simulation package for strong gravitational lensing. *arXiv preprint arXiv:2102.02830*, 2021.
- [43] Masamune Oguri. Strong gravitational lensing of explosive transients. *Reports on Progress in Physics*, 82(12):126901, 2019.
- [44] Aaron Oord, Yazhe Li, Igor Babuschkin, Karen Simonyan, Oriol Vinyals, Koray Kavukcuoglu, George Driessche, Edward Lockhart, Luis Cobo, Florian Stimberg, et al. Parallel wavenet: Fast high-fidelity speech synthesis. In *International conference on machine learning*, pages 3918–3926. PMLR, 2018.
- [45] Ji Won Park. Strongly-lensed quasar selection based on both multi-band tabular data. Project report of the “CS230 Deep Learning” (2018 edition) course at Stanford.
- [46] Ji Won Park, Ashley Villar, Yin Li, Yan-Fei Jiang, Shirley Ho, Joshua Yao-Yu Lin, Philip J Marshall, and Aaron Roodman. Inferring black hole properties from astronomical multivariate time series with bayesian attentive neural processes. *arXiv preprint arXiv:2106.01450*, 2021.
- [47] Milad Pourrahmani, Hooshang Nayyeri, and Asantha Cooray. LensFlow: A convolutional neural network in search of strong gravitational lenses. *The Astrophysical Journal*, 856(1):68, mar 2018.

- [48] Anna M Quider, Max Pettini, Alice E Shapley, and Charles C Steidel. The ultraviolet spectrum of the gravitationally lensed galaxy ‘the Cosmic Horseshoe’: a close-up of a star-forming galaxy at $z \approx 2$. *Monthly Notices of the Royal Astronomical Society*, 398(3):1263–1278, 2009.
- [49] Md Rahman, Thasin Abedin, Khondokar SS Prottoy, Ayana Moshruha, Fazlul Hasan Siddiqui, et al. Semantically Sensible Video Captioning (SSVC). *arXiv preprint arXiv:2009.07335*, 2020.
- [50] Dhanesh Ramachandram and Graham W Taylor. Deep multimodal learning: A survey on recent advances and trends. *IEEE signal processing magazine*, 34(6):96–108, 2017.
- [51] Namiko Saito, Tetsuya Ogata, Satoshi Funabashi, Hiroki Mori, and Shigeki Sugano. How to select and use tools?: Active perception of target objects using multimodal deep learning. *IEEE Robotics and Automation Letters*, 6(2):2517–2524, 2021.
- [52] DP Schneider, JE Gunn, and JG Hoessel. CCD photometry of Abell clusters. I-magnitudes and redshifts for 84 brightest cluster galaxies. *The Astrophysical Journal*, 264:337–355, 1983.
- [53] Rajibul Shaikh, Pritam Banerjee, Suvankar Paul, and Tapobrata Sarkar. Strong gravitational lensing by wormholes. *Journal of Cosmology and Astroparticle Physics*, 2019(07):028, 2019.
- [54] Jonathan Shen, Ruoming Pang, Ron J Weiss, Mike Schuster, Navdeep Jaitly, Zongheng Yang, Zhifeng Chen, Yu Zhang, Yuxuan Wang, Rj Skerrv-Ryan, et al. Natural tts synthesis by conditioning wavenet on mel spectrogram predictions. In *2018 IEEE international conference on acoustics, speech and signal processing (ICASSP)*, pages 4779–4783. IEEE, 2018.
- [55] Hideyuki Shimizu and Keiichi I Nakayama. Artificial intelligence in oncology. *Cancer science*, 111(5):1452–1460, 2020.
- [56] Sören Richard Stahlschmidt, Benjamin Ulfenborg, and Jane Synnnergren. Multimodal deep learning for biomedical data fusion: a review. *Briefings in Bioinformatics*, 23(2), 01 2022. bbab569.
- [57] Brian Stalder, Kevin Reil, Chuck Claver, Ming Liang, Tei Wei Tsai, Travis Lange, Justine Haupt, Oliver Wiccha, Margaux Lopez, Gary Poczulpl, et al. Rubin commissioning camera: integration, functional testing, and lab performance. In *Ground-based and Airborne Instrumentation for Astronomy VIII*, volume 11447, pages 86–98. SPIE, 2020.
- [58] Jabeen Summaira, Xi Li, Amin Muhammad Shoib, Songyuan Li, and Jabbar Abdul. Recent advances and trends in multimodal deep learning: A review. *arXiv preprint arXiv:2105.11087*, 2021.
- [59] Liang Tang, Shunong Zhang, Xuesong Yang, and Shuli Hu. Research on prognosis for engines by LSTM deep learning method. In *2019 Prognostics and System Health Management Conference (PHM-Qingdao)*, pages 1–8. IEEE, 2019.
- [60] Zhiyuan Tang, Ying Shi, Dong Wang, Yang Feng, and Shiyue Zhang. Memory visualization for gated recurrent neural networks in speech recognition. In *2017 IEEE International Conference on Acoustics, Speech and Signal Processing (ICASSP)*, pages 2736–2740. IEEE, 2017.
- [61] Hossen Teimoorinia, Robert D Toyonaga, Sebastien Fabbro, and Connor Bottrell. Comparison of multi-class and binary classification machine learning models in identifying strong gravitational lenses. *Publications of the Astronomical Society of the Pacific*, 132(1010):044501, 2020.
- [62] Rocio Nahime Torres, Piero Fraternali, and Jesus Romero. ODIN: An object detection and instance segmentation diagnosis framework. In *European Conference on Computer Vision*, pages 19–31. Springer, 2020.
- [63] Rocio Nahime Torres, Federico Milani, and Piero Fraternali. ODIN: Pluggable meta-annotations and metrics for the diagnosis of classification and localization. In *International Conference on Machine Learning, Optimization, and Data Science*, pages 383–398. Springer, 2021.
- [64] Tommaso Treu. Strong lensing by galaxies. *Annual Review of Astronomy and Astrophysics*, 48(1):87–125, 2010.
- [65] J Anthony Tyson, F Valdes, and RA Wenk. Detection of systematic gravitational lens galaxy image alignments-mapping dark matter in galaxy clusters. *The Astrophysical Journal*, 349:L1–L4, 1990.
- [66] V Vakulik, R Schild, V Dudinov, S Nuritdinov, V Tsvetkova, O Burkhonov, and T Akhunov. Observational determination of the time delays in gravitational lens system Q2237+ 0305. *Astronomy & Astrophysics*, 447(3):905–913, 2006.
- [67] Riza Velioglu and Jewgeni Rose. Detecting hate speech in memes using multimodal deep learning approaches: Prize-winning solution to hateful memes challenge. *arXiv preprint arXiv:2012.12975*, 2020.
- [68] Marco Vicedomini, Massimo Brescia, Stefano Cavuoti, Giuseppe Riccio, and Giuseppe Longo. *Statistical Characterization and Classification of Astronomical Transients with Machine Learning in the era of the Vera C. Rubin Observatory*, pages 81–113. Springer International Publishing, Cham, 2021.
- [69] Ran Wei, Li Mi, Yaosi Hu, and Zhenzhong Chen. Exploiting the local temporal information for video captioning. *Journal of Visual Communication and Image Representation*, 67:102751, 2020.
- [70] Yiwei Wei, Leiquan Wang, Haiwen Cao, Mingwen Shao, and Chunlei Wu. Multi-attention generative adversarial network for image captioning. *Neurocomputing*, 387:91–99, 2020.
- [71] Radosław Wojtak, Jens Hjorth, and Christa Gall. Magnified or multiply imaged? – Search strategies for gravitationally lensed supernovae in wide-field surveys. *Monthly Notices of the Royal Astronomical Society*, 487(3):3342–3355, 06 2019.
- [72] Tao Xu, Han Zhang, Xiaolei Huang, Shaoting Zhang, and Dimitris N. Metaxas. Multimodal deep learning for cervical dysplasia diagnosis. In Sebastien Ourselin, Leo Joskowicz, Mert R. Sabuncu, Gozde Unal, and William Wells, editors, *Medical Image Computing and Computer-Assisted Intervention – MICCAI 2016*, pages 115–123. Cham, 2016. Springer International Publishing.
- [73] Shudong Yang, Xueying Yu, and Ying Zhou. LSTM and GRU neural network performance comparison study: Taking yelp review dataset as an example. In *2020 International Workshop on Electronic Communication and Artificial Intelligence (IWECAI)*, pages 98–101, 2020.
- [74] Niccolò Zangrando. The ODIN framework, a tool for image classification diagnosis, 2021.
- [75] Fritz Zwicky. On the probability of detecting nebulae which act as gravitational lenses. *Physical Review*, 51(8):679, 1937.

VI. BIOGRAPHY



Nicolò Oreste Pinciroli Vago received the MSc in Computer Science and Engineering at Politecnico di Milano, Italy, and the MSc in Simulation and Visualization at NTNU i Ålesund, Norway, in 2021. He is a research fellow at Politecnico di Milano, in the field of Artificial Intelligence. He is working on the application of Deep Learning to artworks analysis and astrophysics.



Piero Fraternali is full professor of Web Technologies at Politecnico di Milano. Author of more than 200 papers in international peer-reviewed conferences and journals (H index 45) and of four international books. His main research interests concern methodologies and tools for WEB/mobile application development, socio-technical system design, gamification and serious games. He is author of several articles on International Journals and Conference Proceedings, and a number of books. He is co-author of OMG’s IFML standard and cofounder of WebRatio, a start-up focused on the commercialization of a tool suite for the Model-Driven Development of Web/mobile cloud-powered applications.